Longitudinal omics in Syrian hamsters integrated with human data unravel complexity of moderate immune responses to SARS-CoV-2

Supplementary Figures and Tables

Geraldine Nouailles[1,2+*], Emanuel Wyler[3+*], Peter Pennitz[1], Dylan Postmus[2,4], Daria Vladimirova[5], Julia Kazmierski[2,4], Fabian Pott[2,4], Kristina Dietert[6,7], Michael Mülleder[8], Vadim Farztdinov[8], Benedikt Obermayer[9], Sandra-Maria Wienhold[1], Sandro Andreotti[10], Thomas Höfler[5], Birgit Sawitzki[11], Christian Drosten[4], Leif Erik Sander[12], Norbert Suttorp[12], Markus Ralser[13], Dieter Beule[9], Achim Dieter Gruber[6], Christine Goffinet[2,4], Markus Landthaler[14], Jakob Trimpert[5#*] and Martin Witzenrath[1,12,15#*]

+ shared first authorship with equal contributions

# shared senior authorship with equal contributions

* Corresponding authors:

Correspondence to Geraldine Nouailles (geraldine.nouailles@charite.de), Emanuel Wyler (emanuel.wyler@mdc-berlin.de), Jakob Trimpert (jakob.trimpert@fu-berlin.de), Martin Witzenrath (martin.witzenrath@charite.de)

[1] Division of Pulmonary Inflammation, Charité - Universitätsmedizin Berlin, corporate member of Freie Universität Berlin, Humboldt-Universität zu Berlin, and Berlin Institute of Health, Berlin, Germany.

[2] Berlin Institute of Health (BIH), Berlin, Germany.

[3] Berlin Institute for Medical Systems Biology (BIMSB), Max Delbrück Center for Molecular Medicine in the Helmholtz Association (MDC), Berlin, Germany.

[4] Institute of Virology, Charité - Universitätsmedizin Berlin, corporate member of Freie Universität Berlin, Humboldt-Universität zu Berlin and Berlin Institute of Health (BIH), Berlin, Germany.

[5] Institute of Virology, Freie Universität Berlin, Berlin, Germany.

[6] Institute of Veterinary Pathology, Freie Universität Berlin, Berlin, Germany.

[7] Veterinary Centre for Resistance Research, Freie Universität Berlin, Berlin, Germany.

[8] Core Facility - High-Throughput Mass Spectrometry, Charité - Universitätsmedizin Berlin, corporate member of Freie Universität Berlin, Humboldt-Universität zu Berlin and Berlin Institute of Health (BIH), Berlin, Germany.

[9] Core Unit Bioinformatics, Berlin Institute of Health (BIH), Max Delbrück Center for Molecular Medicine in the Helmholtz Association (MDC) and Charité - Universitätsmedizin, Berlin, Germany.
[10] Bioinformatics Solution Center, Freie Universität Berlin, Berlin, Germany.
[11] Institute of Medical Immunology. Charité - Universitätsmedizin Berlin, corporate member of Freie Universität Berlin, Humboldt-Universität zu Berlin, and Berlin Institute of Health, Berlin, Germany.
[12] Department of Infectious Diseases and Respiratory Medicine, Charité - Universitätsmedizin Berlin, corporate member of Freie Universität Berlin, Humboldt-Universität zu Berlin, and Berlin Institute of Health, Berlin, Germany.
[13] The Francis Crick Institute, Molecular Biology of Metabolism Laboratory, London, UK; Department of Biochemistry, Charité - Universitätsmedizin Berlin, corporate member of Freie Universität Berlin, Humboldt-Universität zu Berlin and Berlin Institute of Health (BIH), Berlin, Germany.
[14] Berlin Institute for Medical Systems Biology (BIMSB), Max Delbrück Center for Molecular Medicine in the Helmholtz Association (MDC), Berlin, Germany; IRI Life Sciences, Institute for Biology, Humboldt University Berlin, Berlin, Germany.
[15] German Center for Lung Research (DZL), Berlin, Germany.

Figure S1

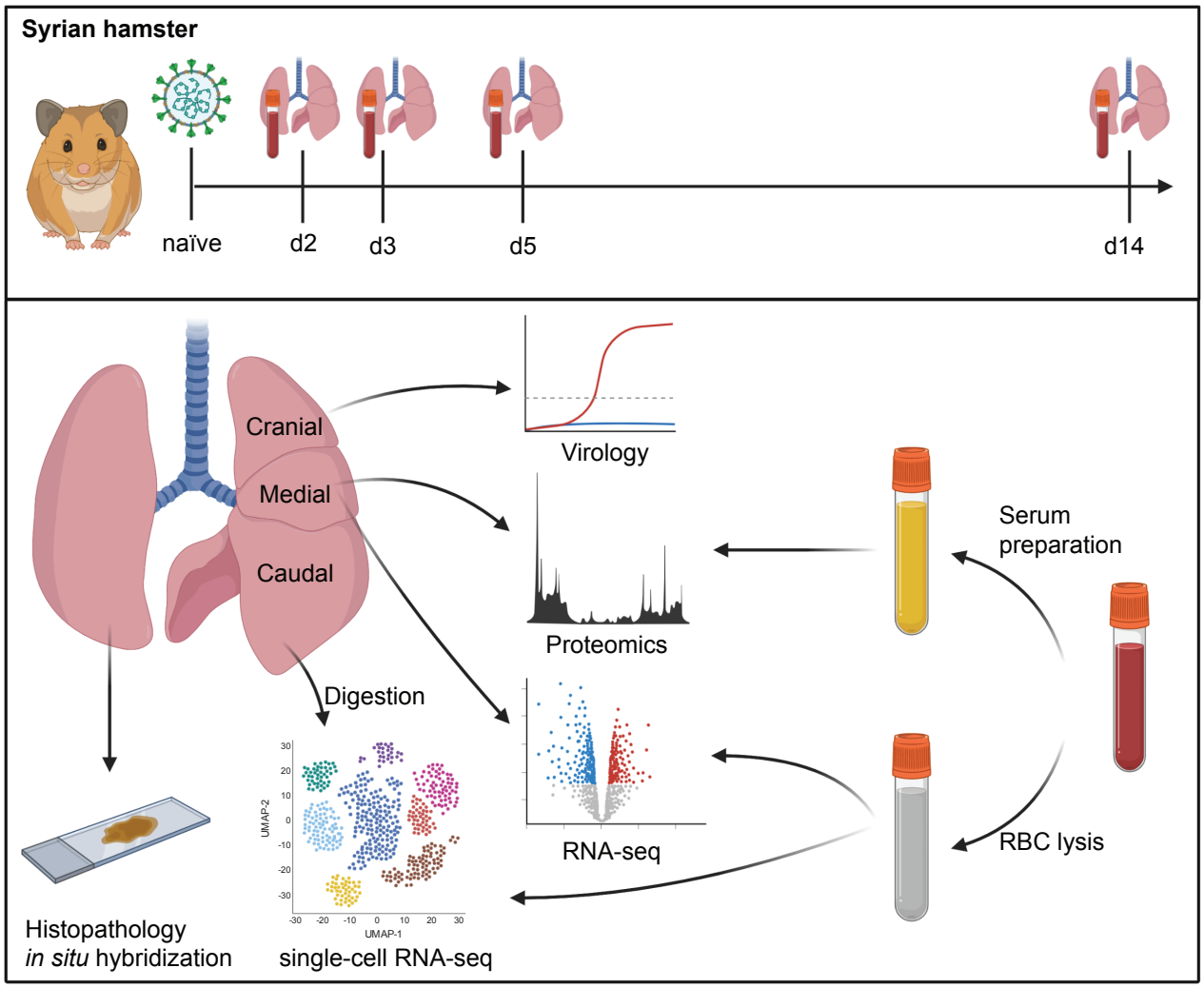

Supplementary Figure 1: Experimental Design

Figure S2

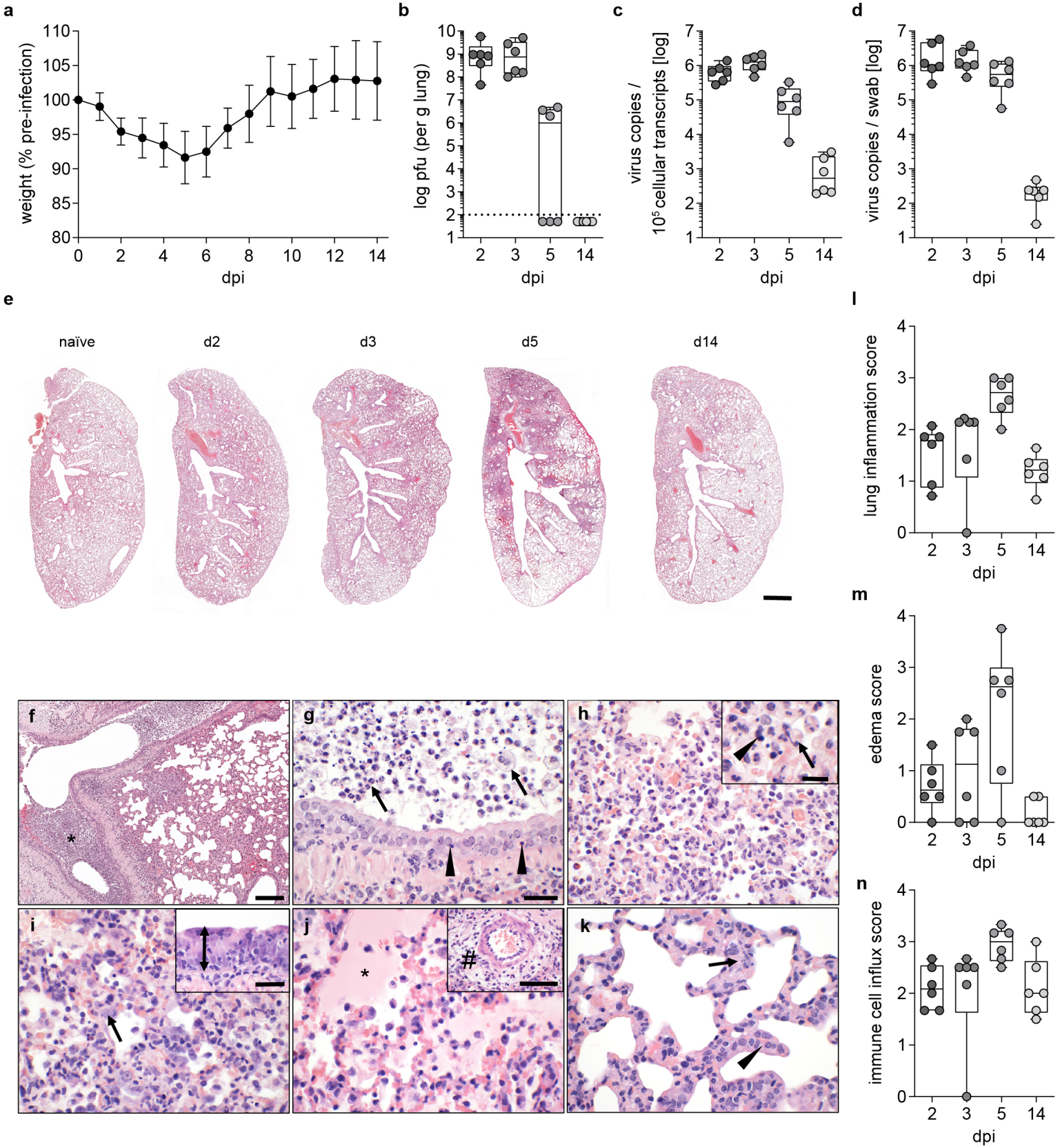

Supplementary Figure 2: Course of SARS-CoV-2 infection in Syrian hamsters. (a), Relative body weight curve of hamsters recorded up to 14 days post infection (dpi). (b), Virus titers in lung homogenates titrated on Vero E6 cells. Dotted line represents limit of detection. (c), SARS-CoV-2 genomic RNA copies in lung tissue per 105 cellular Rpl18 transcripts and (d), RNA copies per bucco-pharyngeal swab. (e), whole cross sectional scans of left lung lobes of naïve (left) or SARS-CoV-2 infected hamsters at 2 to 14 dpi. Bar: 1 mm. (f-k), Histopathology at higher magnifications (representative images of haematoxylin and eosin stains) identified suppurative bronchitis at 2 dpi (f, asterisks) with intraluminal neutrophils (g, arrows) and early bronchointerstitial pneumonia with necrosis of bronchial epithelial cells at 3 dpi (g, arrowheads). At 3 dpi, high numbers of neutrophils and macrophages in alveolar lumina of peripheral lung parenchyma (h; inset: neutrophils, arrowhead and macrophages, arrow). At 5 dpi (i), stronger immune cell influxes accompanied by hyperplasia of alveolar (arrows) and bronchial epithelial cells (inset, double headed arrow). Alveolar (j, asterisk) and perivascular edema (j inset, hash) at 5 dpi. (k) At 14 dpi, inflammation still present albeit weaker, hyperplasia of alveolar epithelial cells, clearance of alveolar edema and re-ventilation of alveolar lumina. f = 200 µm, g – k = 50 µm, inset h = 20 µm, inset i = 50 µm, inset j = 100 µm. (l - n) histopathology scores: parameters were classified (0 absent – 4 severe) and summarized as published (Osterrieder et al., 2020; Schauer et al., 2017) with modifications: (l), lung inflammation score including: severity of pulmonary inflammation, bronchitis, bronchial necrosis, alveolar necrosis, hyperplasia of alveolar epithelial cells type II, bronchial epithelial hyperplasia and endothelitis. (m), edema score: alveolar and perivascular edema. (n), immune cell influx: neutrophils, macrophages and lymphocytes. (a) Mean ± standard deviation (SD), (b – d) and (l – n), Boxplots depicting median, individual values and whiskers (minimum to maximum), n = 6 per time point. (b, d and e), * $p < 0.05$, ** $p < 0.01$, *** $p < 0.001$, **** $p < 0.0001$.

Figure S3, part 1

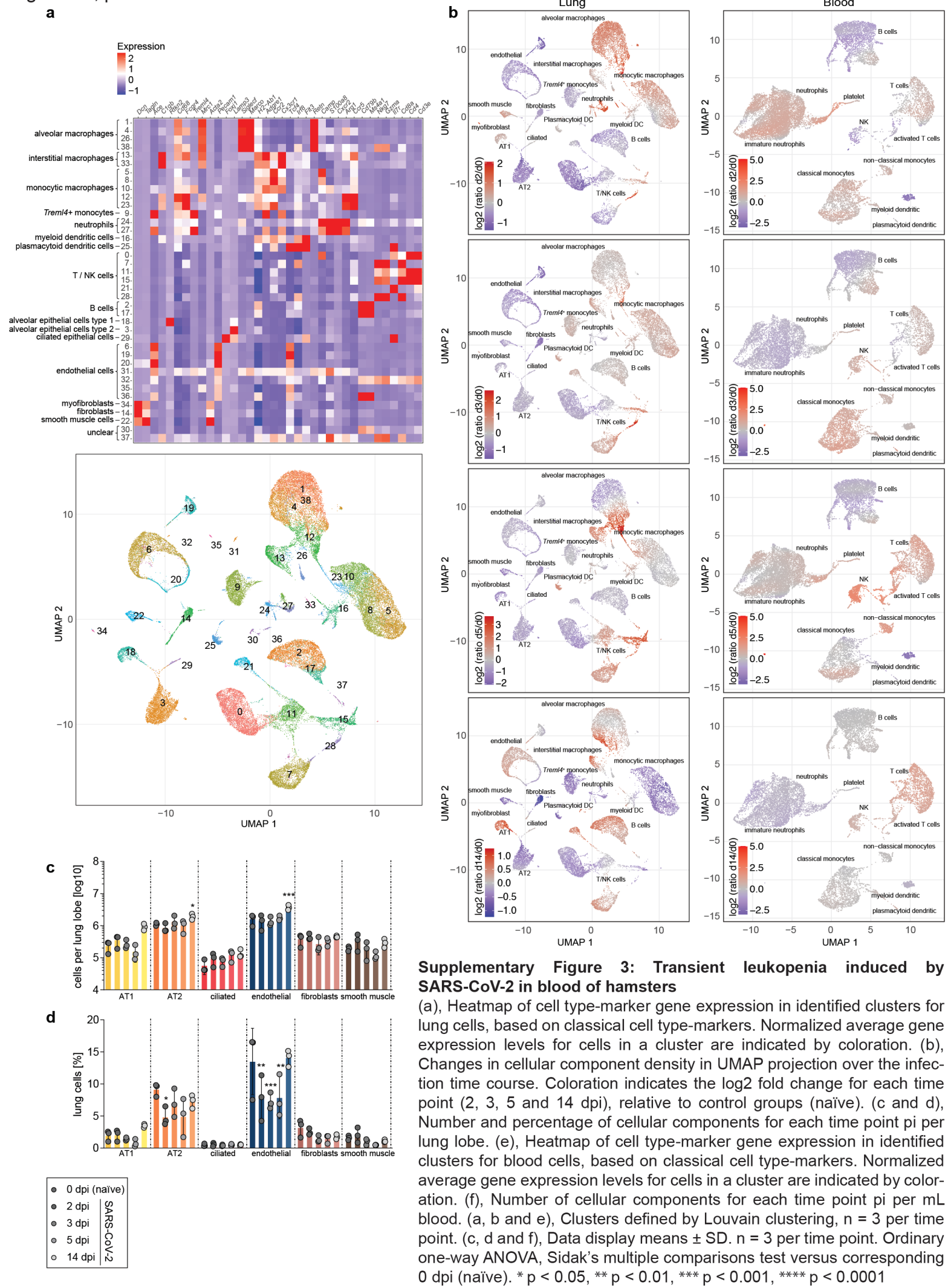

Supplementary Figure 3: Transient leukopenia induced by SARS-CoV-2 in blood of hamsters

(a), Heatmap of cell type-marker gene expression in identified clusters for lung cells, based on classical cell type-markers. Normalized average gene expression levels for cells in a cluster are indicated by coloration. (b), Changes in cellular component density in UMAP projection over the infection time course. Coloration indicates the log2 fold change for each time point (2, 3, 5 and 14 dpi), relative to control groups (naïve). (c and d), Number and percentage of cellular components for each time point pi per lung lobe. (e), Heatmap of cell type-marker gene expression in identified clusters for blood cells, based on classical cell type-markers. Normalized average gene expression levels for cells in a cluster are indicated by coloration. (f), Number of cellular components for each time point pi per mL blood. (a, b and e), Clusters defined by Louvain clustering, n = 3 per time point. (c, d and f), Data display means ± SD. n = 3 per time point. Ordinary one-way ANOVA, Sidak's multiple comparisons test versus corresponding 0 dpi (naïve). * p < 0.05, ** p < 0.01, *** p < 0.001, **** p < 0.0001

Figure S3, part 2

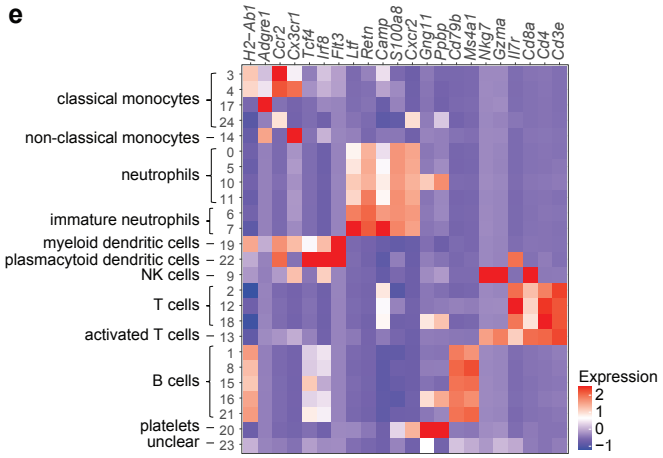

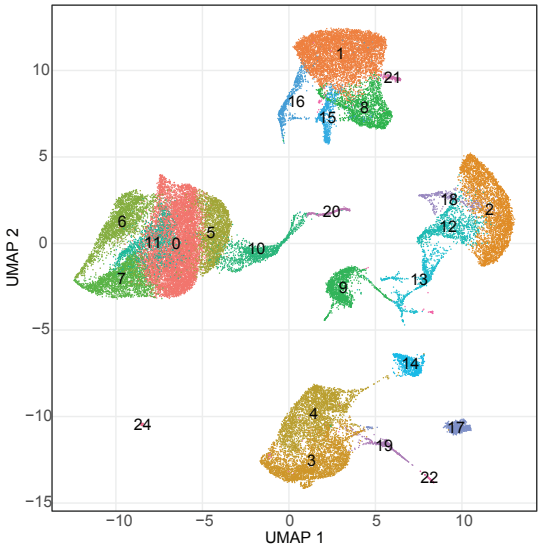

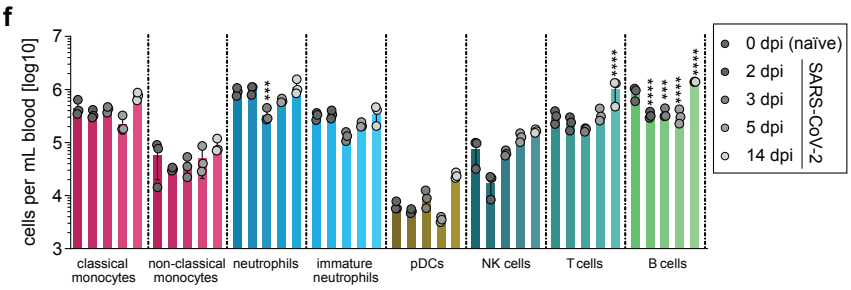

Figure S4 part 1

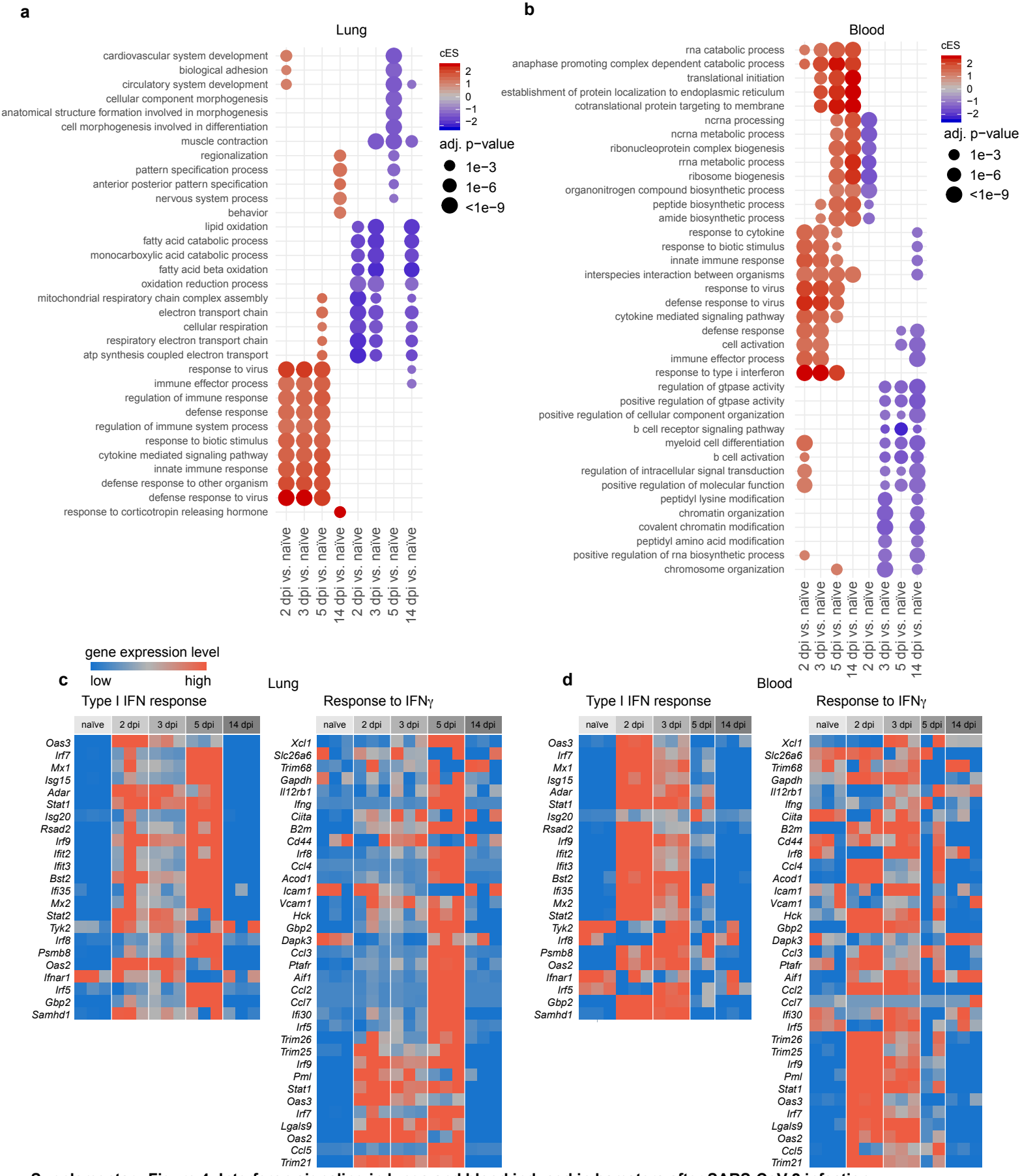

Supplementary Figure 4: Interferon signaling in lungs and blood induced in hamsters after SARS-CoV-2 infection
(a), Dotplot of enriched terms from hallmark, reactome and gene ontology (biological process) gene sets in lung bulk RNA-sequencing samples over the infection time course compared to naïve animals. Coloration and point size indicate effect size and P value for each time point (2, 3, 5 and 14 days post infection, pi), relative to control groups (naïve), as calculated by tmod. (b), as in (a) but for blood samples. (c), Heatmap of interferon type I and interferon gamma related genes as in (Winkler et al., 2020) in lungs over the infection time course. Normalized average gene expression levels (z-scores) are indicated by coloration for each animal. (d), as in (c), but for blood samples. Normalized average gene expression levels are indicated by coloration for each animal, n = 2 for blood samples of day 5 pi, n = 3 for all other time points. (e) Magnitude of host response over time as fraction (in %) of differentially regulated proteins (p-values < 0.01). (f), Correspondence of differentially expressed genes in proteomic and bulk RNA sequencing data was explored by linear regression (intersection at 0) of log transformed fold changes of infected vs control (5 dpi, p.value < 0.01). Linear fit showed almost ideal consistensy between regulations (slope = 0.8) and a correlation coefficient r = 0.9 (r2 = 0.82).

Figure S4 part 2

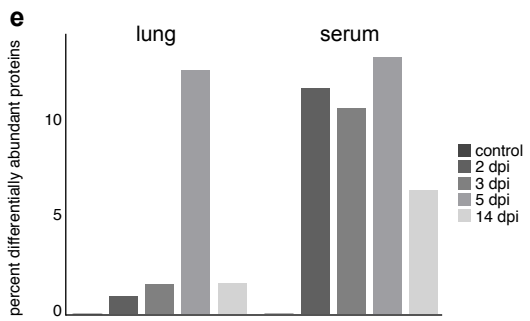

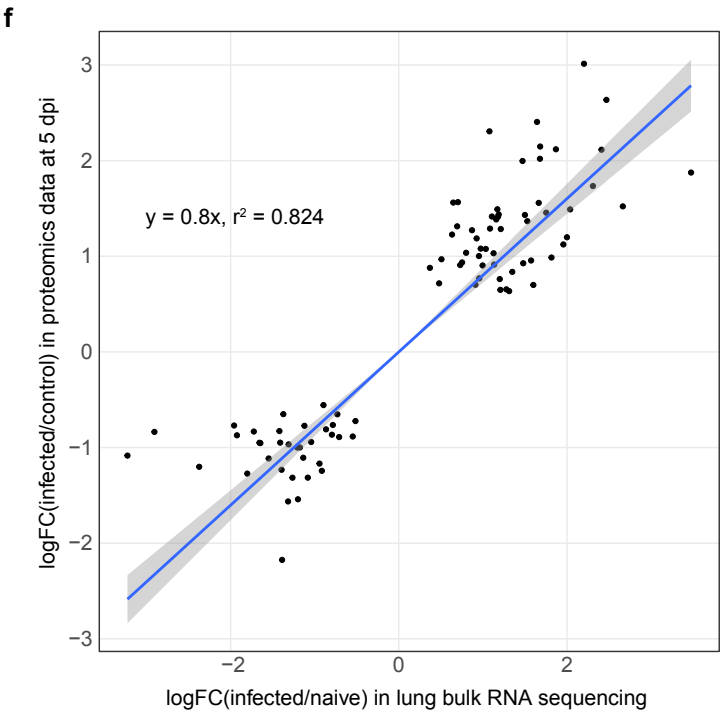

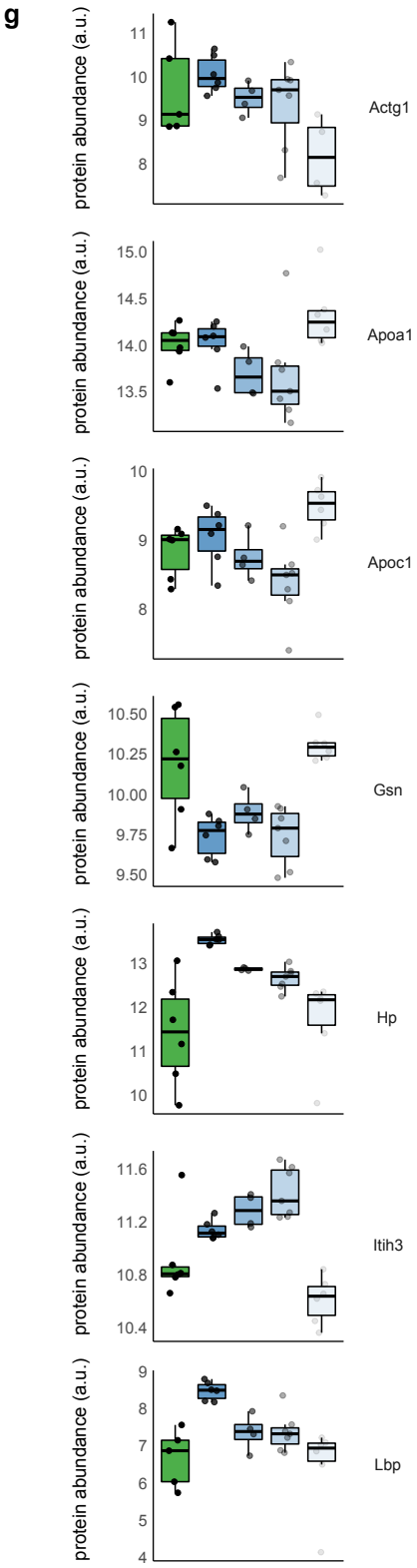

Figure S5, part 1

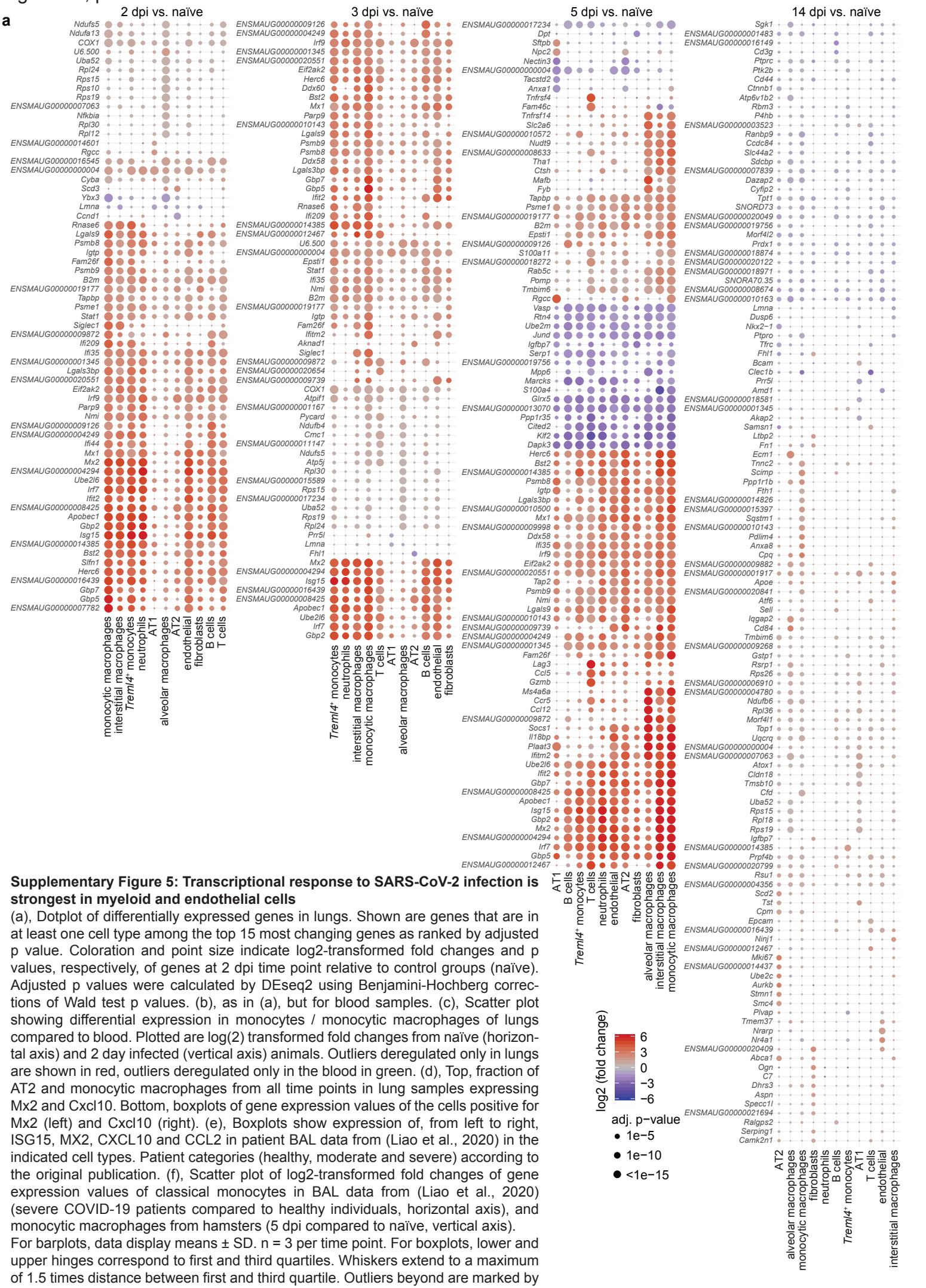

Supplementary Figure 5: Transcriptional response to SARS-CoV-2 infection is strongest in myeloid and endothelial cells

(a), Dotplot of differentially expressed genes in lungs. Shown are genes that are in at least one cell type among the top 15 most changing genes as ranked by adjusted p value. Coloration and point size indicate log2-transformed fold changes and p values, respectively, of genes at 2 dpi time point relative to control groups (naïve). Adjusted p values were calculated by DEseq2 using Benjamini-Hochberg corrections of Wald test p values. (b), as in (a), but for blood samples. (c), Scatter plot showing differential expression in monocytes / monocytic macrophages of lungs compared to blood. Plotted are log(2) transformed fold changes from naïve (horizontal axis) and 2 day infected (vertical axis) animals. Outliers deregulated only in lungs are shown in red, outliers deregulated only in the blood in green. (d), Top, fraction of AT2 and monocytic macrophages from all time points in lung samples expressing Mx2 and Cxcl10. Bottom, boxplots of gene expression values of the cells positive for Mx2 (left) and Cxcl10 (right). (e), Boxplots show expression of, from left to right, ISG15, MX2, CXCL10 and CCL2 in patient BAL data from (Liao et al., 2020) in the indicated cell types. Patient categories (healthy, moderate and severe) according to the original publication. (f), Scatter plot of log2-transformed fold changes of gene expression values of classical monocytes in BAL data from (Liao et al., 2020) (severe COVID-19 patients compared to healthy individuals, horizontal axis), and monocytic macrophages from hamsters (5 dpi compared to naïve, vertical axis).

For barplots, data display means ± SD. n = 3 per time point. For boxplots, lower and upper hinges correspond to first and third quartiles. Whiskers extend to a maximum of 1.5 times distance between first and third quartile. Outliers beyond are marked by single dots.

Figure S5, part 2

b

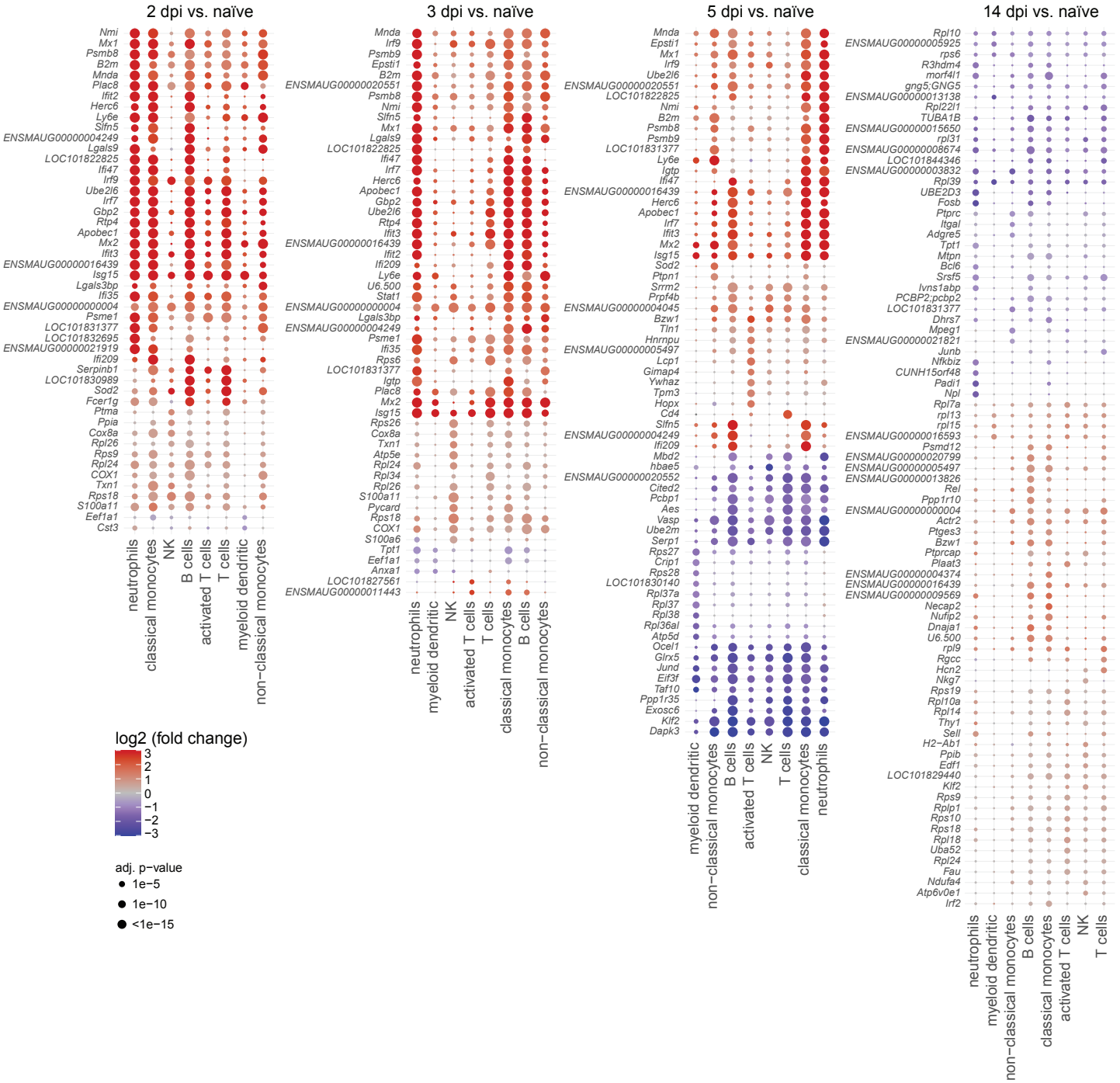

Figure S5, part 3

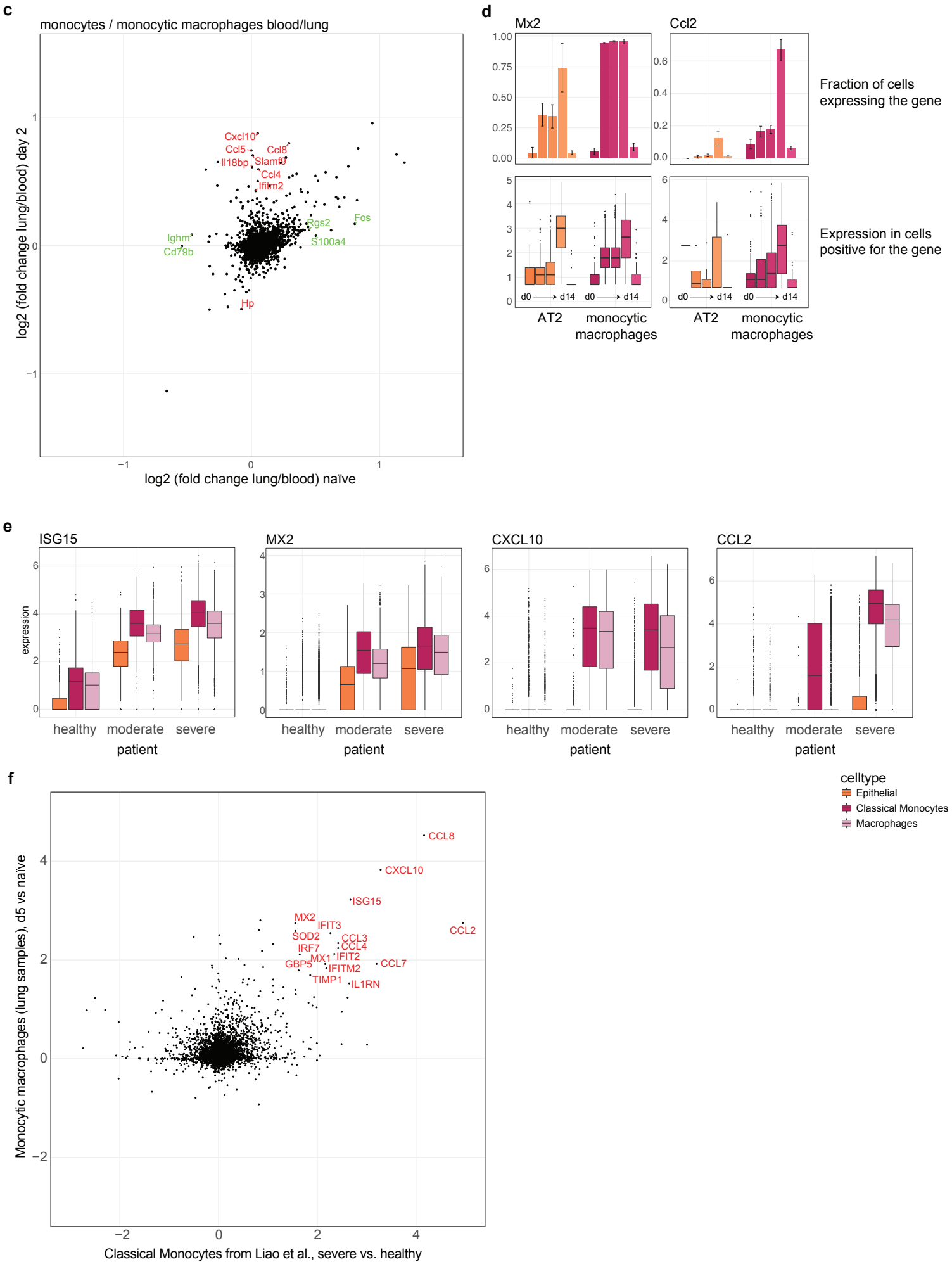

Figure S6

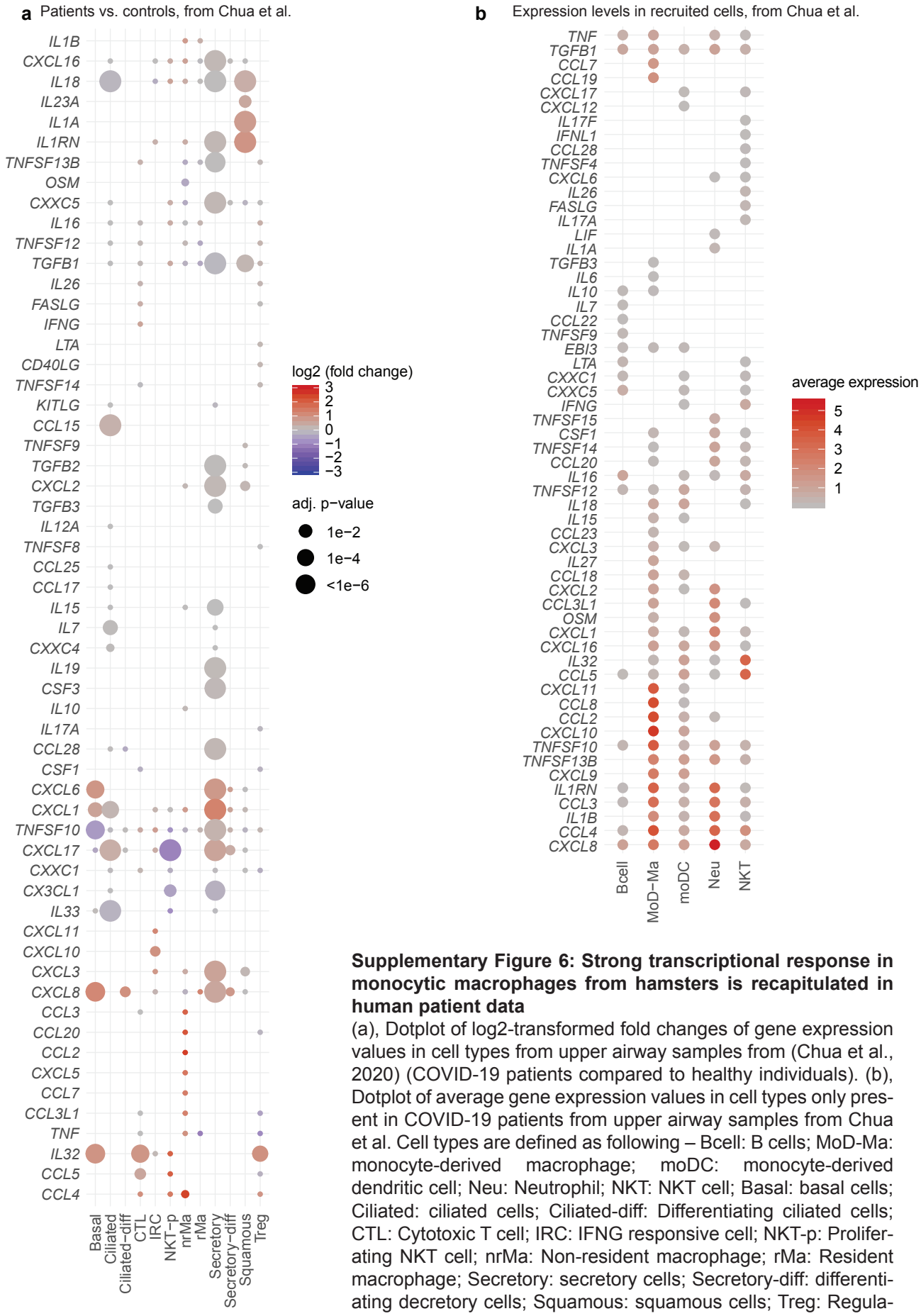

Supplementary Figure 6: Strong transcriptional response in monocytic macrophages from hamsters is recapitulated in human patient data

(a), Dotplot of log2-transformed fold changes of gene expression values in cell types from upper airway samples from (Chua et al., 2020) (COVID-19 patients compared to healthy individuals). (b), Dotplot of average gene expression values in cell types only present in COVID-19 patients from upper airway samples from Chua et al. Cell types are defined as following – Bcell: B cells; MoD-Ma: monocyte-derived macrophage; moDC: monocyte-derived dendritic cell; Neu: Neutrophil; NKT: NKT cell; Basal: basal cells; Ciliated: ciliated cells; Ciliated-diff: Differentiating ciliated cells; CTL: Cytotoxic T cell; IRC: IFNG responsive cell; NKT-p: Proliferating NKT cell; nrMa: Non-resident macrophage; rMa: Resident macrophage; Secretory: secretory cells; Secretory-diff: differentiating decretory cells; Squamous: squamous cells; Treg: Regulatory T cell.

Figure S7

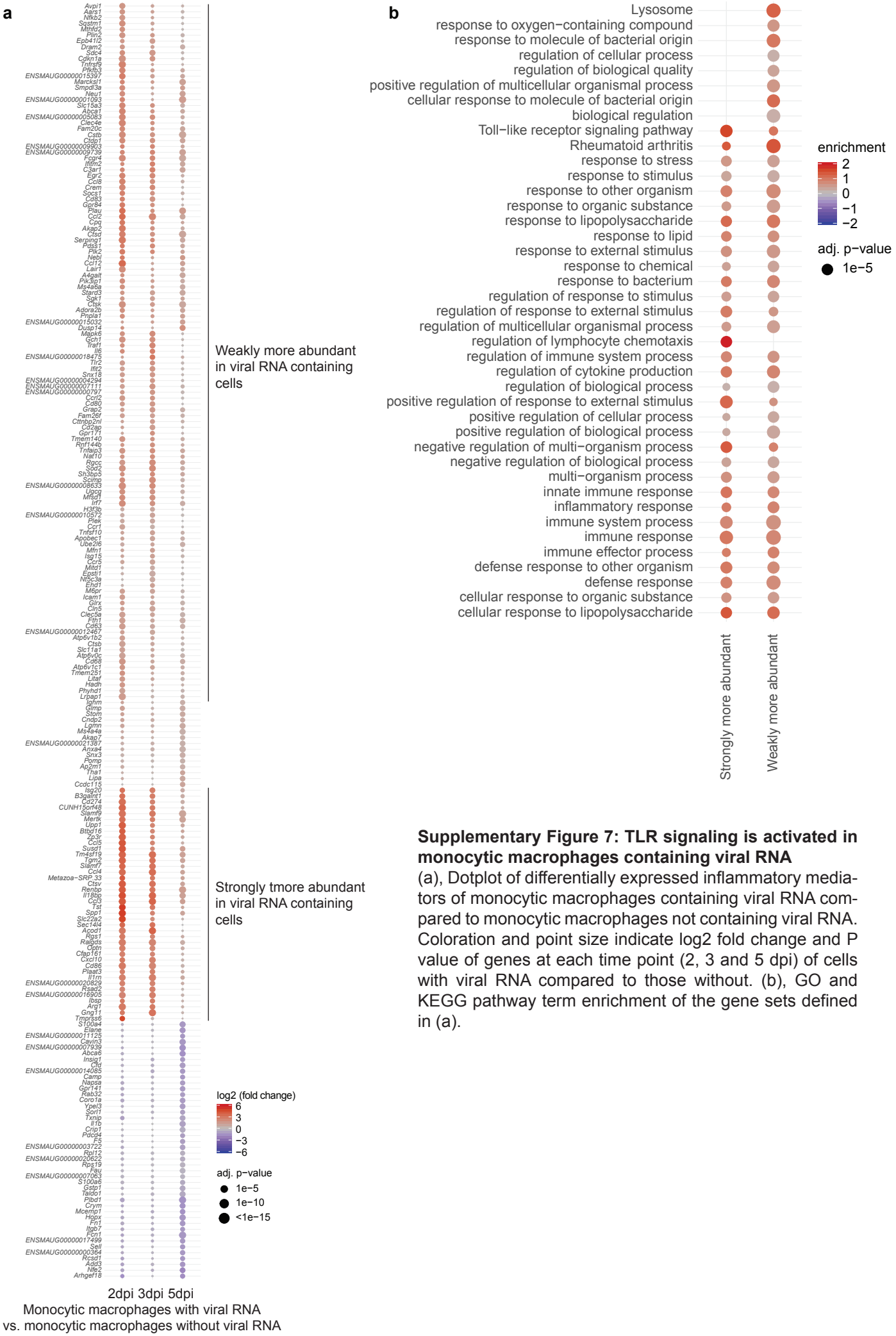

Supplementary Figure 7: TLR signaling is activated in monocytic macrophages containing viral RNA
(a), Dotplot of differentially expressed inflammatory mediators of monocytic macrophages containing viral RNA compared to monocytic macrophages not containing viral RNA. Coloration and point size indicate log2 fold change and P value of genes at each time point (2, 3 and 5 dpi) of cells with viral RNA compared to those without. (b), GO and KEGG pathway term enrichment of the gene sets defined in (a).

Figure S8

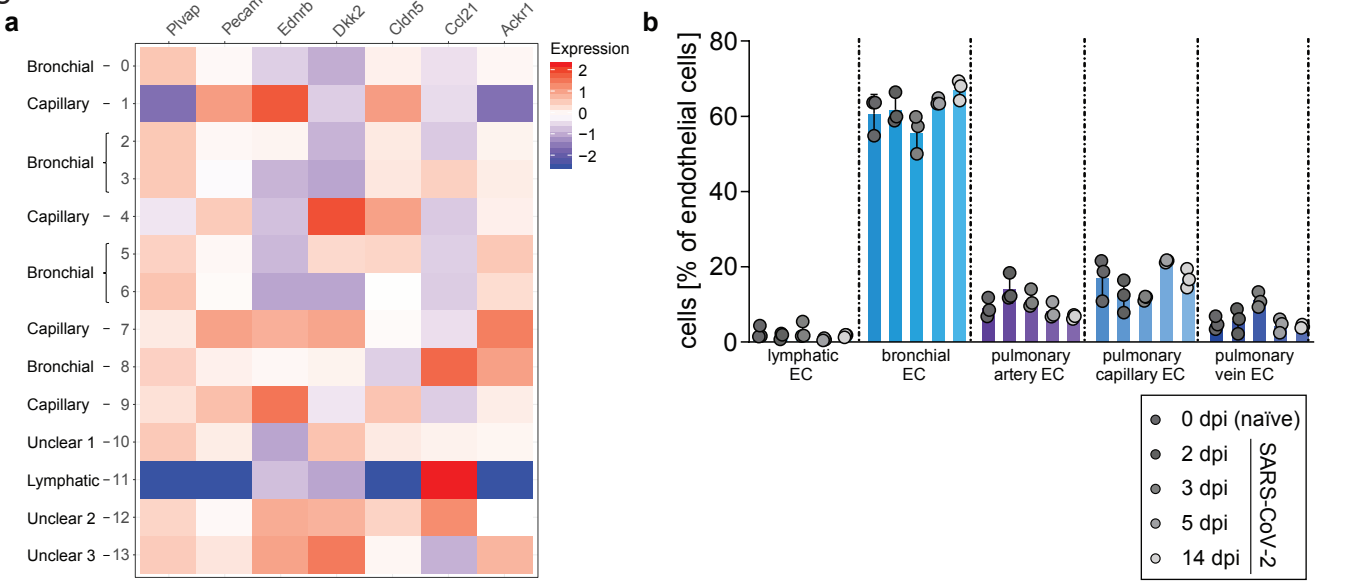

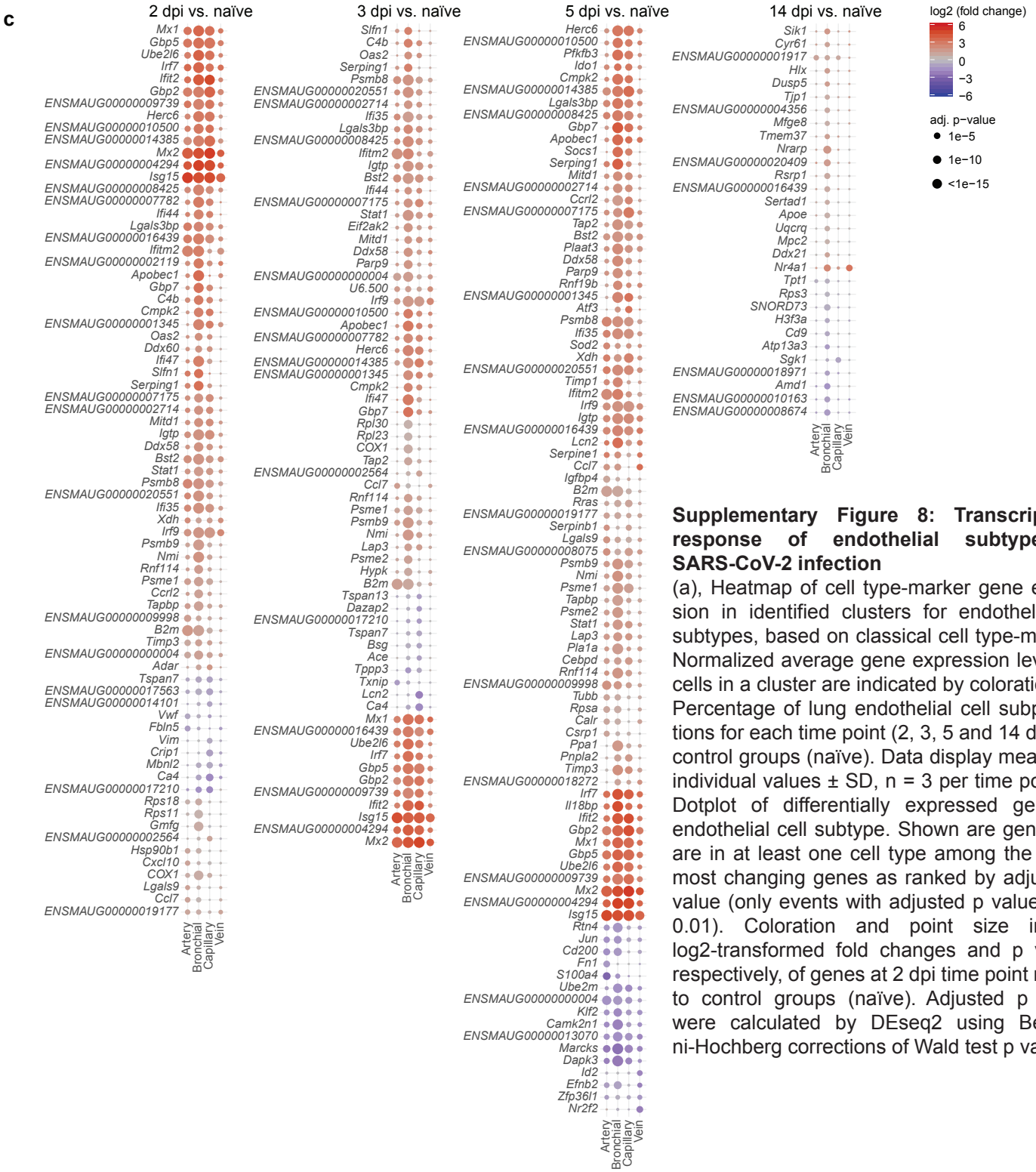

Supplementary Figure 8: Transcriptional response of endothelial subtypes to SARS-CoV-2 infection

(a), Heatmap of cell type-marker gene expression in identified clusters for endothelial cell subtypes, based on classical cell type-markers. Normalized average gene expression levels for cells in a cluster are indicated by coloration. (b), Percentage of lung endothelial cell subpopulations for each time point (2, 3, 5 and 14 dpi) and control groups (naïve). Data display means and individual values ± SD, n = 3 per time point. (c) Dotplot of differentially expressed genes in endothelial cell subtype. Shown are genes that are in at least one cell type among the top 50 most changing genes as ranked by adjusted p value (only events with adjusted p value larger 0.01). Coloration and point size indicate log2-transformed fold changes and p values, respectively, of genes at 2 dpi time point relative to control groups (naïve). Adjusted p values were calculated by DEseq2 using Benjamini-Hochberg corrections of Wald test p values.

Figure S9

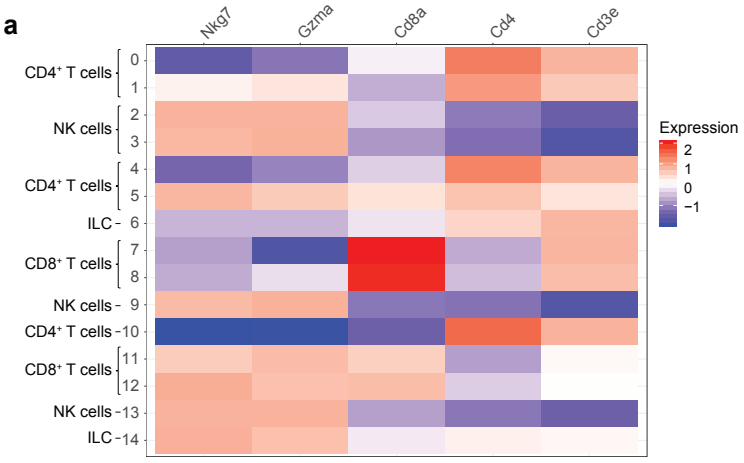

Supplementary Figure 9: Transcriptional response of T and NK cells to SARS-CoV-2 infection
(a), Heatmap of cell type-marker gene expression in identified clusters for T and NK cell subtypes, based on classical cell type-markers. Normalized average gene expression levels for cells in a cluster are indicated by coloration. (b) Dotplot of differentially expressed genes in T and NK cell subtype. Shown are genes that are in at least one cell type among the top 50 most changing genes as ranked by adjusted p value (only events with adjusted p value larger 0.01). Coloration and point size indicate log2-transformed fold changes and p values, respectively. Adjusted p values were calculated by DEseq2 using Benjamini-Hochberg corrections of Wald test p values.

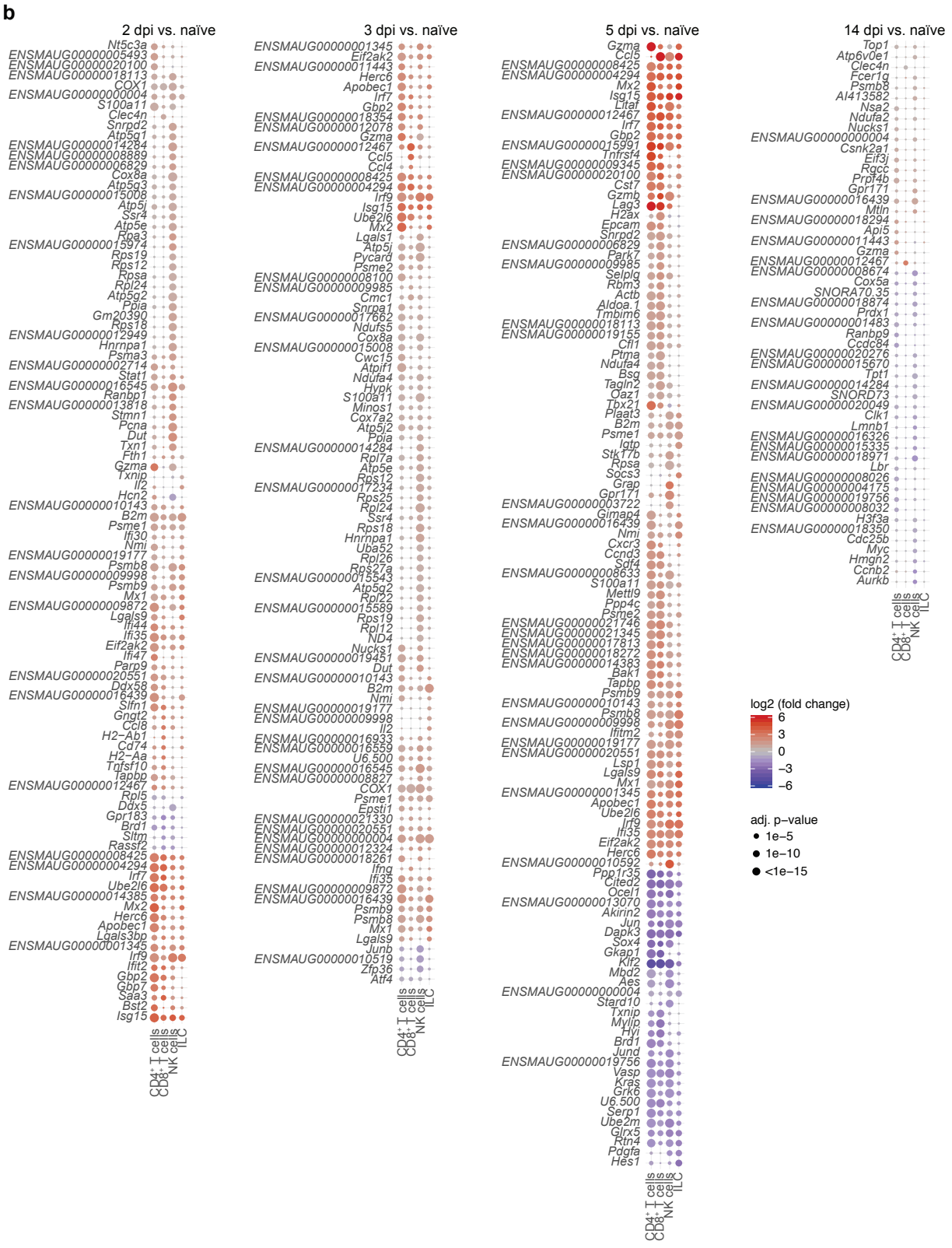

Table S1: Oligonucleotides used in this study.

Primer/probe	**Sequence 5'–3'**
SARS-CoV-2 forward	ACAGGTACGTTAATAGTTAATAGCGT
SARS-CoV-2 reverse	ATATTGCAGCAGTACGCACACA
SARS-CoV-2 probe	FAM-ACACTAGCCATCCTTACTGCGCTTCG-BHQ
RPL-18 forward	GTTTATGAGTCGCACTAACCG
RPL-18 reverse	TGTTCTCTCGGCCAGGAA
RPL-18 probe	FAM-TCTGTCCCTGTCCCGGATGATC-BHQ

Table S2. Identified proteins in respective proteome analysis

Differentially regulated in lung and reported to be regulated in human BAL fluid (22 proteins)		Showing the same direction of change (10 proteins)	Differentially regulated proteins in lung that have been reported to be regulated in human plasma (13 proteins)
Sept11	Ctsz	Sept11	C4b
Sod2	Grb2	Sod2	Ace
Hspa5	Eif6	Hspa5	S100a8
Tppp3	Gprc5a	Tppp3	Serpind1
Galm	Rps19	Galm	Ighm
Csrp1	Lap3	Csrp1	Hp
Dpysl2	Cd9	Dpysl2	B2m
Vat1	Samhd1	Vat1	Hpx
Igkv7-33	Aqp5	Igkv7-33	Itih3
Lgals3bp		Lgals3bp	Serping1
Cotl1			Igkv7-33
Pls3			Cfi
Psme1			Lgals3bp

Showing the same trend (9 proteins)	Differentially expressed in serum (37 proteins)		Proteins reported in human COVID19 studies (20 proteins)	
S100a8	Apoc1	Cfd	Apoc1	Actg1
Ighm	Cetp	Aldh1a1	C4b	
Hp	C4b	Pon1	Gsn	
B2m	Smco3		C6	
Itih3	Gsn	Apoc3	Apoa1	
Serping1	C6	Mbl1	Clu	
Igkv7-33	Apoa1	Clec3b	Serping1	
Cfi	Hbae5	Hpx	Hp	
Lgals3bp	Igkv7-33		Hpx	
	Clu	Hbb-y	Lbp	
	Serping1	Agt	Itih3	
	Hp	Calb1	Rbp4	
	Adipoq	Actg1	Ttr	
	Dusp2	Amy1	Cfd	
	Pltp	Aldob	Pon1	
	Cndp1	ENSMAUG00000021094	Apoc3	
	Lbp	ENSMAUG00000016284	Clec3b	
	Itih3	ENSMAUG00000001023	Igkv7-33	
	Rbp4	ENSMAUG00000004376	Agt	
	Ttr			

Table S3. Frequencies of *Ace2*, *Tmprss2*, *Furin*, *Bsg*, *Nrp1, Ext1* mRNA–positive and SARS-CoV-2 positive cell populations.

Gene	Day (d)	Alveolar epithelial cells type 1	Alveolar epithelial cells type 2	Ciliated epithelial cells	Endothelial cells	Fibroblasts	Alveolar macrophages	Monocytic macrophages	Interstitial macrophages
Ace2	0 dpi (naïve)	0.43±0.74	3.70±1.20	21.82±13.73	0.06±0.11	0.00	1.10±0.36	0.28±0.34	1.38±1.59
	2 dpi	0.98±1.70	3.79±1.00	4.44±7.70	0.00	0.00	1.09±0.58	0.30±0.19	0.50±0.86
	3 dpi	0.67±1.15	3.53±1.24	10.13±8.77	0.00	0.00	0.90±0.23	0.23±0.21	0.46±0.80
	5 dpi	0.00	4.83±1.52	0.00	0.00	0.00	0.14±0.25	0.25±0.16	1.10±1.28
	14 dpi	1.85±1.89	4.60±0.75	7.25±2.38	0.00	0.00	1.15±0.61	0.09±0.15	0.69±1.20
Tmprss2	0 dpi (naïve)	73.68±5.59	12.00±1.86	34.55±14.43	0.13±0.11	0.00	0.00	0.06±0.11	0.00
	2 dpi	44.91±8.72	5.76±0.66	27.29±14.75	0.11±0.19	0.00	0.07±0.12	0.24±0.26	0.00
	3 dpi	54.25±5.04	9.30±1.66	27.14±5.45	0.00	0.50±0.86	0.13±0.11	0.09±0.08	0.00
	5 dpi	56.19±18.23	11.98±2.16	6.58±7.93	0.00	0.00	0.14±0.25	0.08±0.07	0.00
	14 dpi	65.57±6.49	15.43±0.53	30.98±11.78	0.36±0.23	0.00	0.10±0.18	0.00	0.00
Furin	0 dpi (naïve)	30.63±1.02	16.55±3.07	29.29±9.74	18.95±1.20	10.50±5.86	10.21±2.47	25.95±1.46	18.75±6.56
	2 dpi	28.69±6.20	16.74±3.98	31.00±8.89	17.28±0.91	18.77±2.99	13.57±2.99	23.90±6.26	16.45±6.63
	3 dpi	34.97±4.62	22.97±2.42	26.24±9.55	19.09±0.99	16.61±8.21	12.58±1.10	28.69±0.55	19.72±5.95
	5 dpi	24.11±12.96	22.74±5.35	6.58±7.93	22.19±0.79	17.62±2.39	40.03±9.12	52.76±4.78	51.63±1.61
	14 dpi	30.71±5.03	20.67±1.69	42.16±11.14	19.31±0.91	14.13±5.82	12.32±4.06	26.70±5.07	25.16±8.76
Bsg	0 dpi (naïve)	100.0±0.00	93.93±1.35	96.97±5.25	94.36±3.50	96.07±2.40	95.10±1.37	76.55±7.16	83.81±3.96
	2 dpi	99.49±0.89	90.65±4.77	95.21±4.18	92.69±5.16	96.92±2.07	92.28±4.19	77.19±7.13	84.03±9.83
	3 dpi	98.73±1.11	92.80±0.95	96.30±6.42	95.12±2.42	98.71±1.20	93.39±1.62	80.17±1.03	85.90±2.87
	5 dpi	100.00±0.00	99.46±0.93	92.34±7.20	99.24±1.10	100.00±0.00	91.50±2.72	92.23±1.11	97.43±1.53
	14 dpi	99.70±0.52	97.71±0.62	98.04±3.40	98.11±1.55	100.00±0.00	97.28±0.82	87.00±2.76	95.36±2.10
Nrp1	0 dpi (naïve)	0.44±0.76	32.06±6.04	4.14±4.60	54.92±10.61	12.65±3.25	0.25±0.44	1.40±0.65	7.81±7.34
	2 dpi	0.90±0.80	32.99±5.15	1.28±2.22	45.48±9.69	10.75±5.14	0.22±0.37	2.18±0.98	6.43±4.89
	3 dpi	0.95±1.65	41.46±7.27	1.67±2.89	57.70±5.56	19.76±12.25	0.32±0.56	1.97±0.68	6.98±2.44
	5 dpi	0.72±1.26	35.24±4.96	8.96±5.74	55.25±8.27	10.16±5.77	12.33±6.84	16.66±2.06	34.58±15.48
	14 dpi	1.74±0.78	35.94±2.55	0.00	68.53±2.41	25.47±8.05	0.30±0.05	1.86±0.29	9.47±2.81
Ext1	0 dpi (naïve)	22.43±3.37	12.37±1.46	5.25±4.71	8.14±1.62	20.62±6.23	17.74±2.64	6.81±1.25	8.14±1.20
	2 dpi	12.66±5.06	9.73±3.97	9.97±11.29	7.38±3.38	17.89±4.81	11.46±2.73	7.48±1.39	8.75±4.24
	3 dpi	17.70±7.72	12.37±1.85	33.65±20.33	11.76±0.53	35.84±12.53	16.41±2.84	12.86±1.65	10.97±2.54
	5 dpi	19.89±7.84	15.24±5.47	8.36±8.71	9.06±1.21	25.12±0.59	22.93±5.25	27.84±1.82	27.74±4.85
	14 dpi	20.68±3.15	10.34±2.58	7.25±6.34	10.73±2.82	37.87±7.61	10.20±3.68	5.73±1.72	7.75±0.82
SARS-Cov-2	2 dpi	6.01±7.89	6.41±6.55	6.07±5.79	4.95±5.91	4.46±6.70	7.85±6.82	10.24±6.67	9.39±7.33
	3 dpi	10.48±13.31	12.05±6.41	15.50±4.45	9.15±7.70	10.05±6.01	12.20±8.66	11.47±7.40	15.76±11.03
	5 dpi	4.17±7.22	2.76±3.91	7.84±0.79	1.88±1.63	2.14±2.52	24.77±0.31	9.65±2.32	15.74±5.02
	14 dpi	0.00	0.00	0.00	0.00	0.00	0.00	0.00	0.00

[1]Data are represented as mean±standard deviation. *Ace2*, Angiotensin-converting enzyme 2, *Tmprss2,* transmembrane serine protease 2, *Bsg*, Basigin, *Nrp1*, neutropilin, *Ext1* heparan sulfate, SARS-CoV-2, severe acute respiratory syndrome coronavirus 2, dpi, days post infection

Supplementary Figure legends

Supplementary Figure 1: Experimental Design

Supplementary Figure 2: Course of SARS-CoV-2 infection in Syrian hamsters. (a), Relative body weight curve of hamsters recorded up to 14 days post infection (dpi). (b), Virus titers in lung homogenates titrated on Vero E6 cells. Dotted line represents limit of detection. (c), SARS-CoV-2 genomic RNA copies in lung tissue per 10^5 cellular *Rpl18* transcripts and (d), RNA copies per bucco-pharyngeal swab. (e), whole cross sectional scans of left lung lobes of naïve (left) or SARS-CoV-2 infected hamsters at 2 to 14 dpi. Bar: 1 mm. (f-k), Histopathology at higher magnifications (representative images of haematoxylin and eosin stains) identified suppurative bronchitis at 2 dpi (f, asterisks) with intraluminal neutrophils (g, arrows) and early bronchointerstitial pneumonia with necrosis of bronchial epithelial cells at 3 dpi (g, arrowheads). At 3 dpi, high numbers of neutrophils and macrophages in alveolar lumina of peripheral lung parenchyma (h; inset: neutrophils, arrowhead and macrophages, arrow). At 5 dpi (i), stronger immune cell influxes accompanied by hyperplasia of alveolar (arrows) and bronchial epithelial cells (inset, double headed arrow). Alveolar (j, asterisk) and perivascular edema (j inset, hash) at 5 dpi. (k) At 14 dpi, inflammation still present albeit weaker, hyperplasia of alveolar epithelial cells, clearance of alveolar edema and re-ventilation of alveolar lumina. f = 200 µm, g – k = 50 µm, inset h = 20 µm, inset i = 50 µm, inset j = 100 µm. (l - n) histopathology scores: parameters were classified (0 absent – 4 severe) and summarized as published (Osterrieder et al., 2020; Schauer et al., 2017) with modifications: (l), lung inflammation score including: severity of pulmonary inflammation, bronchitis, bronchial necrosis, alveolar necrosis, hyperplasia of alveolar epithelial cells type II, bronchial epithelial hyperplasia and endothelitis. (m), edema score: alveolar and perivascular edema. (n), immune cell influx: neutrophils, macrophages and lymphocytes. (a) Mean ± standard deviation (SD), (b – d) and (l – n), Boxplots depicting median, individual values and whiskers (minimum to maximum), n = 6 per time point. (b, d and e), $*$ $P < 0.05$, $**$ $P < 0.01$, $***$ $P < 0.001$, $****$ $P < 0.0001$.

Supplementary Figure 3: Transient leukopenia induced by SARS-CoV-2 in blood of hamsters

(a), Heatmap of cell type-marker gene expression in identified clusters for lung cells, based on classical cell type-markers. Normalized average gene expression levels for cells in a cluster are indicated by coloration. (b), Changes in cellular component density in UMAP projection over the infection time course. Coloration indicates the log2 fold change for each time point (2, 3, 5 and 14 dpi), relative to control groups (naïve). (c and d), Number and percentage of cellular components for each time point pi per lung lobe. (e), Heatmap of cell type-marker gene expression in identified clusters for blood cells, based on classical cell type-markers. Normalized average gene expression levels for cells in a cluster are indicated by coloration. (f), Number of cellular components for each time point pi per mL blood. (a, b and e), Clusters defined by Louvain clustering, n = 3 per time point. (c, d and f), Data display means ± SD. n = 3 per time point. Ordinary one-way ANOVA, Sidak's multiple comparisons test versus corresponding 0 dpi (naïve). $*$ $p < 0.05$, $**$ $p < 0.01$, $***$ $p < 0.001$, $****$ $p < 0.0001$

Supplementary Figure 4: Interferon signaling in lungs and blood induced in hamsters after SARS-CoV-2 infection

(a), Dotplot of enriched terms from hallmark, reactome and gene ontology (biological process) gene sets in lung bulk RNA-sequencing samples over the infection time course compared to naïve animals. Coloration and point size indicate effect size and *P* value for each time point (2, 3, 5 and 14 days post infection, pi), relative to control groups (naïve), as calculated by tmod. (b), as in (a) but for blood samples. (c), Heatmap of interferon type I and interferon gamma related genes as in (Winkler et al., 2020) in lungs over the infection time course. Normalized average gene expression levels (z-scores) are indicated by coloration for each animal. (d), as in (c), but for blood samples. Normalized average gene expression levels are indicated by coloration for each animal, n = 2 for blood samples of day 5 pi, n = 3 for all other time points. (e) Magnitude of host response over time as fraction (in %) of differentially regulated proteins (p-values < 0.01). (f), Correspondence of differentially expressed genes in proteomic and bulk RNA sequencing data was explored by linear regression (intersection at 0) of log transformed fold changes of infected vs control (5 dpi, p.value < 0.01). Linear fit showed almost ideal consistensy between regulations (slope = 0.8) and a correlation coefficient r = 0.9 (r2 = 0.82).

Supplementary Figure 5: Transcriptional response to SARS-CoV-2 infection is strongest in myeloid and endothelial cells

(a), Dotplot of differentially expressed genes in lungs. Shown are genes that are in at least one cell type among the top 15 most changing genes as ranked by adjusted *p* value. Coloration and point size indicate log2-transformed fold changes and *p* values, respectively, of genes at 2 dpi time point relative to control groups (naïve). Adjusted *p* values were calculated by DEseq2 using Benjamini-Hochberg corrections of Wald test *p* values. (b), as in (a), but for blood samples. (c), Scatter plot showing differential expression in monocytes / monocytic macrophages of lungs compared to blood. Plotted are log(2) transformed fold changes from naïve (horizontal axis) and 2 day infected (vertical axis) animals. Outliers deregulated only in lungs are shown in red, outliers deregulated only in the blood in green. (d), Top, fraction of AT2 and monocytic macrophages from all time points in lung samples expressing *Mx2* and *Cxcl10*. Bottom, boxplots of gene expression values of the cells positive for *Mx2* (left) and *Cxcl10* (right). (e), Boxplots show expression of, from left to right, *ISG15*, *MX2*, *CXCL10* and *CCL2* in patient BAL data from (Liao et al., 2020) in the indicated cell types. Patient categories (healthy, moderate and severe) according to the original publication. (f), Scatter plot of log2-transformed fold changes of gene expression values of classical monocytes in BAL data from (Liao et al., 2020) (severe COVID-19 patients compared to healthy individuals, horizontal axis), and monocytic macrophages from hamsters (5 dpi compared to naïve, vertical axis).

For barplots, data display means ± SD. n = 3 per time point. For boxplots, lower and upper hinges correspond to first and third quartiles. Whiskers extend to a maximum of 1.5 times distance between first and third quartile. Outliers beyond are marked by single dots.

Supplementary Figure 6: Strong transcriptional response in monocytic macrophages from hamsters is recapitulated in human patient data

(a), Dotplot of log2-transformed fold changes of gene expression values in cell types from upper airway samples from (Chua et al., 2020) (COVID-19 patients compared to healthy individuals). (b), Dotplot of average gene expression values in cell types only present in COVID-19 patients from upper airway samples from Chua et al. Cell types are defined as following – Bcell: B cells; MoD-Ma: monocyte-derived macrophage;

moDC: monocyte-derived dendritic cell; Neu: Neutrophil; NKT: NKT cell; Basal: basal cells; Ciliated: ciliated cells; Ciliated-diff: Differentiating ciliated cells; CTL: Cytotoxic T cell; IRC: IFNG responsive cell; NKT-p: Proliferating NKT cell; nrMa: Non-resident macrophage; rMa: Resident macrophage; Secretory: secretory cells; Secretory-diff: differentiating decretory cells; Squamous: squamous cells; Treg: Regulatory T cell.

Supplementary Figure 7: TLR signaling is activated in monocytic macrophages containing viral RNA

(a), Dotplot of differentially expressed inflammatory mediators of monocytic macrophages containing viral RNA compared to monocytic macrophages not containing viral RNA. Coloration and point size indicate log2 fold change and *P* value of genes at each time point (2, 3 and 5 dpi) of cells with viral RNA compared to those without. (b), GO and KEGG pathway term enrichment of the gene sets defined in (a).

Supplementary Figure 8: Transcriptional response of endothelial subtypes to SARS-CoV-2 infection

(a), Heatmap of cell type-marker gene expression in identified clusters for endothelial cell subtypes, based on classical cell type-markers. Normalized average gene expression levels for cells in a cluster are indicated by coloration. (b), Percentage of lung endothelial cell subpopulations for each time point (2, 3, 5 and 14 dpi) and control groups (naïve). Data display means and individual values ± SD, n = 3 per time point. (c) Dotplot of differentially expressed genes in endothelial cell subtype. Shown are genes that are in at least one cell type among the top 50 most changing genes as ranked by adjusted *p* value (only events with adjusted *p* value larger 0.01). Coloration and point size indicate log2-transformed fold changes and *p* values, respectively, of genes at 2 dpi time point relative to control groups (naïve). Adjusted *p* values were calculated by DEseq2 using Benjamini-Hochberg corrections of Wald test *p* values.

Supplementary Figure 9: Transcriptional response of T and NK cells to SARS-CoV-2 infection

(a), Heatmap of cell type-marker gene expression in identified clusters for T and NK cell subtypes, based on classical cell type-markers. Normalized average gene expression levels for cells in a cluster are indicated by coloration. (b) Dotplot of differentially expressed genes in T and NK cell subtype. Shown are genes that are in

at least one cell type among the top 50 most changing genes as ranked by adjusted *p* value (only events with adjusted *p* value larger 0.01). Coloration and point size indicate log2-transformed fold changes and *p* values, respectively. Adjusted *p* values were calculated by DEseq2 using Benjamini-Hochberg corrections of Wald test *p* values.

Supplementary Table 1: Oligonucleotides used in this study

Supplementary Table 2: Specific protein sets referenced in the proteomics results

Supplementary Table 3: Frequencies of cell types positive for the virus or specified genes